

# Feature Extraction for DW-MRI Visualization: The State of the Art and Beyond\*

Thomas Schultz

Computer Science Department and Computation Institute  
University of Chicago, USA  
t.schultz@uchicago.edu

---

## Abstract

By measuring the anisotropic self-diffusion rates of water, Diffusion Weighted Magnetic Resonance Imaging (DW-MRI) provides a unique noninvasive probe of fibrous tissue. In particular, it has been explored widely for imaging nerve fiber tracts in the human brain. Geometric features provide a quick visual overview of the complex datasets that arise from DW-MRI. At the same time, they build a bridge towards quantitative analysis, by extracting explicit representations of structures in the data that are relevant to specific research questions. Therefore, features in DW-MRI data are an active research topic not only within scientific visualization, but have received considerable interest from the medical image analysis, neuroimaging, and computer vision communities. It is the goal of this paper to survey contributions from all these fields, concentrating on streamline clustering, edge detection and segmentation, topological methods, and extraction of anisotropy creases. We point out interrelations between these topics and make suggestions for future research.

**1998 ACM Subject Classification** I.3.8 [Computer Graphics]: Applications; I.4.6 [Image Processing and Computer Vision]: Segmentation; I.5.3 [Pattern Recognition]: Clustering; J.3 [Computer Applications]: Life and Medical Sciences

**Keywords and phrases** Diffusion-Weighted MRI, dMRI, DT-MRI, DTI, HARDI, Streamline Clustering, Edge Detection, DW-MRI Segmentation, Tensor Topology, Crease Surfaces

## 1 Introduction

Diffusion-Weighted Magnetic Resonance Imaging (DW-MRI) offers a unique way to investigate the directionally dependent heat motion of water molecules in biological tissue [68]. In nerve fiber bundles or muscles, the diffusion tensor (DT-MRI) model estimates a single principal fiber direction [9]. High angular resolution diffusion imaging (HARDI) allows for even more complex models of apparent diffusion coefficients [90], spin displacement probabilities [122], or fiber densities [118]. Information acquired by DW-MRI is being used, among others, for studying nerve-related disease [48] and normal brain function [104], and for improved planning of brain surgery [134].

Generating visual representations of DW-MRI data has been an active topic in the scientific visualization community in the past decade. Similar to research in flow visualization [97], existing work in this field can be classified as follows:

1. *Direct methods* use simple rules to map data to visual attributes, for example by color mapping [92] or volume rendering [63].

---

\* This work was supported by a fellowship within the Postdoc Program of the German Academic Exchange Service (DAAD).



© Thomas Schultz;

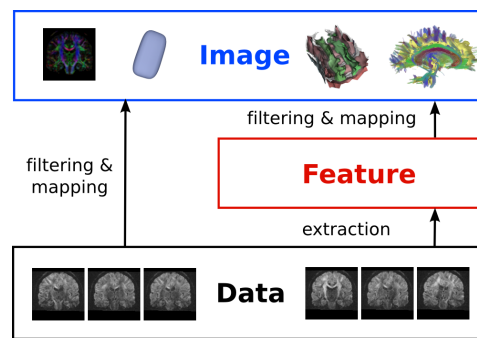
licensed under Creative Commons License NC-ND

To appear in: Proc. Dagstuhl Scientific Visualization Workshop 2009.



DAGSTUHL Dagstuhl Publishing

FOLLOW-UPS Schloss Dagstuhl – Leibniz-Zentrum für Informatik, Germany



■ **Figure 1** Feature extraction introduces an explicit layer of abstraction that reduces DW-MRI data to the relevant information.

2. *Image-based techniques* generate a texture that conveys certain aspects of the data, for example by variants of line integral convolution [49, 141], reaction-diffusion textures [63], or brush strokes [67].
3. *Geometry-based techniques* generate three-dimensional objects that correspond directly to attributes of the data, like streamlines [82, 139] or glyphs [58].
4. *Feature-based visualization* involves an explicit layer of abstraction between the data itself and its visualization (cf. Figure 1, from [105]), and will be the topic of our paper. Feature definitions meet the requirements of specific research questions, and aim to extract non-local structures from the data.

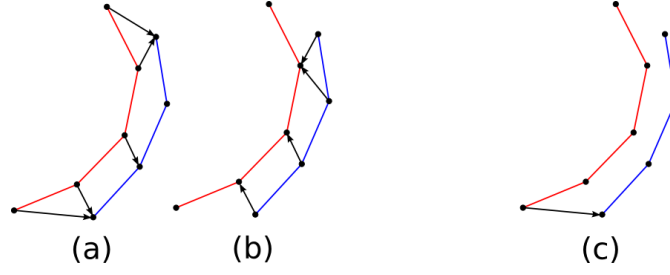
Several book chapters survey DW-MRI visualization in general [98, 123, 140], but they neither focus on feature-based techniques, nor do they reflect the rapid progress that has been made in the last few years. Therefore, it is the goal of our paper to present a panoramic view of the diverse literature on features in DW-MRI data, to include work that has been published outside the visualization community, and to identify directions of future research. We will assume that the reader is familiar with basic concepts of diffusion-weighted data acquisition, preprocessing, modeling, and derived scalar quantities like fractional anisotropy, which are explained in excellent existing surveys [8, 132, 2].

The material has been organized as follows: Section 2 presents features that are based on clustered streamlines. Section 3 reviews algorithms that segment white or gray matter based on edges or uniform regions in DW-MRI data. Section 4 concentrates on topological methods, while Sections 5 treats crease extraction. Finally, Section 6 concludes the paper.

## 2 Streamline Clustering and Visualization of Fiber Bundles

Fiber tracking aims at reconstructing the trajectories of major nerve fiber bundles. In the context of visualization, streamline tractography, which integrates lines tangential to inferred fiber directions, represents the most widely used type of fiber tracking [30, 23, 82, 10]. With the diffusion tensor model, it amounts to streamline integration in the principal eigenvector field. Even though a successful streamline visualization requires suitable termination criteria [83] and strategies for seeding, culling, and rendering [139], these problems are outside the scope of our survey, since they do not pertain to feature extraction in the strict sense.

Streamlines visually convey the inferred fiber bundle trajectories in an intuitive manner. However, even though they are frequently called “fibers”, they do not have clear anatomical correlates: Single axons are far below the imaging resolution, and the full fiber bundles



■ **Figure 2** The mean streamline distance  $d_\mu$  takes an average of the arrow lengths in (a) and (b). The Hausdorff distance  $d_H$  only considers the single longest arrow, shown in (c).

typically comprise more than a single streamline. It is the goal of fiber clustering to group individual streamlines into anatomically more meaningful units, which are referred to as fiber bundles. Given a whole brain tractography, clustering is required to make the sheer amount of streamlines more manageable, and it facilitates more abstract and concise visualizations.

Streamline clustering involves at least three major decisions: Defining a measure of similarity between streamlines, choosing a clustering algorithm, and selecting the desired number of clusters. When multiple datasets are considered simultaneously, an additional challenge is to identify correspondences between subjects.

## 2.1 Distance Measures for Clustering

Some clustering algorithms require a distance measure on pairs of streamlines, while others rely on a similarity measure. In practice, there are various ways to obtain a distance from a similarity and vice versa; a common one is to map high to low values via a Gaussian kernel [16, 86]. For clarity, this section will present all approaches in terms of distance measures.

Most distance measures can be defined in terms of two streamlines  $F_i$  and  $F_j$ , which are given as uniformly sampled polygonal curves with vertices  $\mathbf{p}_k$  and  $\mathbf{p}_l$ , respectively. The most frequent choice is the mean Euclidean distance  $d_\mu$  from all points of one streamline to the other curve, averaged over both lines [116, 26, 80] (cf. Figure 2 (a) and (b)):

$$d_\mu(F_i, F_j) = \frac{1}{2} (\tilde{d}_\mu(F_i, F_j) + \tilde{d}_\mu(F_j, F_i))$$

$$\text{with } \tilde{d}_\mu(F_i, F_j) = \text{mean}_{\mathbf{p}_k \in F_i} \min_{\mathbf{p}_l \in F_j} \|\mathbf{p}_k - \mathbf{p}_l\| \quad (1)$$

For matching streamlines from both hemispheres, O’Donnell and Westin [86] use a variant of  $d_\mu$ , in which they take the minimum of  $\tilde{d}_\mu(F_i, F_j)$  and  $\tilde{d}_\mu(F_j, F_i)$  instead of the average.

Occasionally, the Hausdorff distance  $d_H$  has been considered. It is a “worst case distance”, based on the single point from either line which maximizes the distance to the other streamline (cf. Figure 2 (c)) [26, 80]:

$$d_H(F_i, F_j) = \max(\tilde{d}_H(F_i, F_j), \tilde{d}_H(F_j, F_i))$$

$$\text{with } \tilde{d}_H(F_i, F_j) = \max_{\mathbf{p}_k \in F_i} \min_{\mathbf{p}_l \in F_j} \|\mathbf{p}_k - \mathbf{p}_l\| \quad (2)$$

Zhang et al. [138] take the average over points whose distance to the other streamline is larger than some threshold. This measure is in-between  $d_\mu$  and  $d_H$ , in the sense that it emphasizes diverging parts of the curves more than  $d_\mu$ , but less strongly than  $d_H$ . Some authors have also tried the minimum distance between the streamlines as a measure for clustering, but found that it produces inadequate results, since anatomically distinct tracts frequently pass each other at short distances [26, 80].

In a naive implementation, clustering with the distance measures above involves a comparison of all pairs of points for all pairs of streamlines. Given the length and number of streamlines in full-brain tractography, this quickly becomes prohibitively inefficient. The following strategies have been proposed to reduce the computational burden:

- Ding et al. [33] only consider neighboring pairs of streamlines, and match subsequent vertices on both lines, rather than looking for closest points. However, this requires correct alignment of streamlines, and their algorithm to compute it only works if all fibers were seeded along a common plane.
- Brun et al. [17] define a simpler distance measure, which is based on the streamline endpoints. Moberts et al. [80] find that empirically, this measure produces similar results as the Hausdorff distance, which might indicate that for many pairs of streamlines, the maximum distance occurs near their endpoints.
- In a follow-up, Brun et al. [16] generate a descriptor for each streamline by treating its vertices as a point cloud and computing its mean and the square root of its covariance matrix. Then, streamlines are compared by taking the Euclidean distance of the resulting nine-dimensional feature vectors.
- Xia et al. [135] reduce the problem size by initializing the clustering based on a gray matter atlas. Similarly, Maddah et al. [73] only compute distances from streamlines to cluster representatives, which they initialize manually. An additional speedup is obtained by pre-computing a distance transformation of each representative.
- O’Donnell and Westin [86] use an approximative clustering algorithm that only requires them to compute all pairwise distances within a representative subset of all streamlines. Moreover, they evaluate Equation (1) on subsampled streamline representations.

Even though some convergence towards the use of  $d_\mu$  has been observed [86], it is not entirely settled which measure is the most appropriate, or if different ones should be used depending on the clustering algorithm. Moberts et al. [80] quantify how closely various algorithms and distance measures reproduce a ground truth clustering. In their results, the mean distance  $d_\mu$  consistently performs better than the Hausdorff distance  $d_H$ . However, to our knowledge, there is no systematic comparison available that includes the “in-between” measure by Zhang et al. [138] or the computationally attractive feature-based measure by Brun et al. [16].

Finally, Tsai et al. [121] argue that in order to correctly capture the manifolds on which streamlines lie, the definition of pairwise distances should also take into account the trajectories of all other streamlines. They achieve this by constructing and intersecting minimum spanning trees rooted at each streamline. However, a comparison to traditional distance measures has only been provided on one synthetic example.

## 2.2 Algorithms for Streamline Clustering

The simplest methods for streamline clustering use the nearest neighbor algorithm or some variant of it [33]. Starting with one cluster per streamline, clusters are merged iteratively if at least one pair of streamlines is closer than some distance threshold  $\theta$  [26, 80, 138]. Since nearest neighbor clustering produces a hierarchy of refined clusters for decreasing values of  $\theta$ , it is also called “agglomerative hierarchical clustering” [136].

In nearest neighbor clustering, a single pair of similar streamlines can cause a merge of two otherwise very different clusters. Zhang et al. [138] argue that this helps to cluster sheetlike structures like the corpus callosum. On the other hand, noise in the data can generate spurious streamlines that act as a bridge between anatomically separate clusters

and can cause a false merge. Moberts et al. [80] have experimented with some alternative criteria for cluster merging, but none of them improved the results.

Shimony et al. [116] and Maddah et al. [73] have considered fuzzy clustering algorithms, which quantify the certainty to which a streamline belongs to a bundle. These probabilities were both visualized and used in a statistical tract-based analysis [73]. However, to our knowledge, the practical merit over a quantitative analysis that is based on hard clusters [87] has not been studied systematically.

Brun et al. [16] treat the clustering as a graph cut problem. Representing each streamline by a node in a similarity graph, they search for a bipartition that minimizes the summed similarities of the streamlines that are separated, with a normalization that avoids overly small clusters [115]. Like the nearest neighbor methods, this is a hierarchical technique, but it starts with all streamlines in a single cluster, recursively subdividing it until a threshold or a pre-specified number of clusters is reached. The algorithm has also been employed by Enders et al. [36] and Schultz et al. [111]. O'Donnell and Westin [86] use a variant of it, in which they find k-way graph cuts by k-means clustering in a spectral feature space.

The greedy local approaches used in [26, 80, 138] and the global methods in [116, 16, 86, 73] represent two fundamentally different strategies. Generally, local techniques are simpler to understand and to implement, while global ones are more robust against outliers. To our knowledge, no direct experimental comparison is available. However, only one of the global algorithms [86] has been refined to a point at which the reproducibility of its results over subjects and operators has been quantified [124].

### 2.3 Clustering Parameters

The most important parameter in clustering is the number of desired clusters. In some cases, this parameter is not explicit. Rather, the number of clusters may follow from a desired homogeneity within clusters or a minimum distance between them. In such cases, creating a plot of the number of clusters as a function of the underlying algorithmic parameter can help the user to find the most appropriate value [26].

In theory, such a plot could also be used to try and detect a “natural” clustering implied by the data: Ideally, a clustering that agrees well with the data should remain stable over a considerable range of parameters. To our knowledge, O'Donnell and Westin [86] made the only published attempt to identify the cluster number inherent in the data: Based on a plot of the sum of maximum point-to-centroid distances over the number of clusters, they motivate their choice of 200 clusters for a full-brain tractography.

Moberts et al. [80] use a scoring function to find good parameter values automatically. However, it is defined with respect to a given ground truth clustering, and the authors do not study how well the identified parameters carry over to different datasets for which ground truth may not be known.

At the current state of the art, high-quality streamline clusterings cannot be obtained fully automatically. Therefore, O'Donnell and Westin [86] deliberately generate an oversegmentation, and allow the user to merge clusters manually. Alternatively, Zhang et al. [138] create a user interface for an interactive exploration of the parameter space. As long as streamline clustering requires considerable intervention by an expert, it competes against methods that facilitate a reproducible manual selection of fiber bundles [114, 15, 1]. The frameworks by Chen et al. [21] and Jianu et al. [50] combine both approaches by integrating tools for manual selection in linked two- and three-dimensional views with algorithms for automated clustering.

## 2.4 Clustering of Populations

A preliminary for cross-subject comparison is spatial alignment of the individual datasets. Multi-subject image registration is a field of its own with a rich body of literature [81]. The specific methods that have been used in the context of streamline clustering include block matching (in [74]), congealing (in [86]), and FLIRT (in [138]). Once alignment has been achieved, there are three general strategies to find corresponding clusters between subjects: Joint clustering, explicit matching, and atlas-based.

O'Donnell and Westin [86] take the union of the streamlines from all coregistered datasets and cluster them jointly. This is a conceptually very simple extension of single-subject clustering, and it automatically yields cross-subject correspondences. However, it increases the problem size dramatically. Therefore, O'Donnell and Westin employ several approximations, the most important of them being the Nystrom method for finding normalized graph cuts.

After combining the streamlines from different subjects, tracts are no longer separated clearly enough to apply the nearest neighbor algorithm. Therefore, Zhang et al. [138] perform clustering on individual subjects and determine correspondences explicitly: Each cluster is described by a nine-dimensional feature vector that captures the mean fiber start-, mid- and endpoints, and correspondences are found based on feature similarity.

The final option is to store descriptors of known fiber bundles in an atlas. Then, streamlines from new subjects are simply assigned to one of the predefined clusters. The resulting labeling is not only consistent over subjects, but also identifies specific tracts automatically. To transfer labels from the atlas to new subjects, Maddah et al. [74] use a B-Spline matching to find the most similar streamline, while O'Donnell and Westin [86] represent fibers as points in a high-dimensional feature space, and assign new streamlines to the closest cluster centroid.

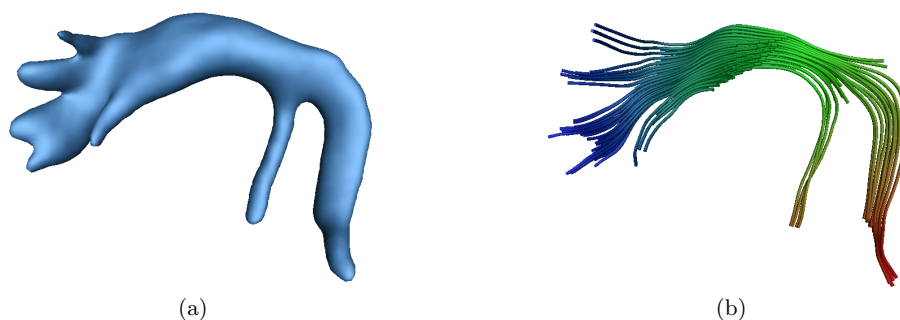
## 2.5 Representing and Rendering Streamline Clusters

Initially, a clustered fiber bundle is represented as a set of sampled streamlines. Mean or medial lines are a more global representation, and can be constructed in various ways [33, 25, 36, 73, 137, 22]. They have been used to establish correspondences between individual fibers, to act as projection targets for diffusion quantities, to extract geometrical measures like curvature and torsion, or to support visualization. Instead of generating a new line to represent the cluster, O'Donnell et al. [87] select the “most typical” existing one.

For applications in surgical planning, it is important to visualize not just the center, but the full spatial extent of a bundle. Enders et al. [36] use a convex hull algorithm to generate envelopes that wrap a variable percentage of streamlines within the bundle. To give an impression of bundle cores and their full extent, surfaces for different parameter choices are overlaid. To handle more complex bundle geometry, such as branchings, different variants of the alpha shape algorithm have been employed by Merhof et al. [78] and by Chen et al. [22]. Based on a statistical model of the bundle, Maddah et al. [73] generate renderings that depict an interval of three standard deviations around the mean fiber, but they do not provide details on their algorithm for surface construction.

Yushkevich et al. [137] and Schultz et al. [107] have estimated the extent of a bundle by rasterizing the streamlines to a voxel grid and applying a small amount of Gaussian blur on the resulting density volume. Merhof et al. [79] have demonstrated that isosurfaces of such volumes (Figure 3 (a)) provide a simple alternative way to obtain fiber hulls.

In neuroscience, streamline clustering is often used as a preprocess for a tract-based statistical analysis of diffusion measures like mean diffusivity or fractional anisotropy. This



■ **Figure 3** Hulls of fiber bundles (a) have been considered for surgical applications. Correspondences between streamlines (shown by same hue in (b)) are needed for streamline-based spatial statistics.

requires correspondences between points on the individual streamlines or, alternatively, a common shape-based coordinate system. In order to establish such correspondences, Ding et al. [33] match the intersection points of individual streamlines and a plane orthogonal to the medial line. Corouge et al. [24] define a cutting plane through the bundle manually, and match points with the same arc length from the resulting intersection points. This strategy was used to create Figure 3 (b). Maddah et al. [73] create a Voronoi diagram of the mean fiber vertices and match streamline vertices that fall into the same Voronoi cell. After a quantitative comparison to these prior methods, O'Donnell et al. [87] decide to compute an optimal point matching using a variant of the Hungarian algorithm [65].

Intra-cluster variations in streamline shape are modeled by Corouge et al. [25], who perform a Procrustes analysis to achieve curve alignment, followed by a Principal Component Analysis of vertex coordinates. Alternatively, Batchelor et al. [11] explore a variety of quantitative measures of curve shape that do not require point-to-point registration.

### 3 Edge Detection and Segmentation

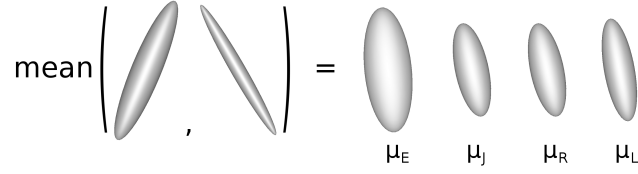
White matter segmentation tries to localize fiber bundles without performing streamline tractography, typically by grouping together regions with similar local diffusion properties, or by growing regions until a boundary is reached. It is also possible to segment some gray matter structures from DW-MRI data. This frequently involves probabilistic tractography as a pre-process.

#### 3.1 Distance Measures for Segmentation

In order to identify voxels with similar diffusion properties, the first step is to choose a distance measure  $d(\mathbf{T}^{(1)}, \mathbf{T}^{(2)})$  for diffusion tensors  $\mathbf{T}$ . Since symmetric  $3 \times 3$  tensors form a six-dimensional vector space, it is possible to simply use the Euclidean metric  $d_E$  on that space [133, 38, 100]. In terms of tensor components  $t_{ij}$ , it is given as

$$d_E(\mathbf{T}^{(1)}, \mathbf{T}^{(2)}) = \sqrt{\sum_{i=1}^3 \sum_{j=1}^3 (t_{ij}^{(1)} - t_{ij}^{(2)})^2} \quad (3)$$

Alternatively, the scalar product  $\langle \mathbf{T}^{(1)}, \mathbf{T}^{(2)} \rangle$  that corresponds to the Euclidean space (i.e.,  $d_E(\mathbf{T}^{(1)}, \mathbf{T}^{(2)}) = \sqrt{\langle \mathbf{T}^{(1)} - \mathbf{T}^{(2)}, \mathbf{T}^{(1)} - \mathbf{T}^{(2)} \rangle}$ ) can serve as a measure of tensor similarity. It is given in terms of tensor components  $t_{ij}$  or, equivalently, in terms of eigenvalues  $\lambda_i$  and



■ **Figure 4** The choice of metric or distance measure changes the definition of the mean tensor.

eigenvectors  $\mathbf{e}_i$ :

$$\langle \mathbf{T}^{(1)}, \mathbf{T}^{(2)} \rangle = \sum_{i=1}^3 \sum_{j=1}^3 t_{ij}^{(1)} t_{ij}^{(2)} = \sum_{i=1}^3 \sum_{j=1}^3 \lambda_i^{(1)} \lambda_j^{(2)} \langle \mathbf{e}_i^{(1)}, \mathbf{e}_j^{(2)} \rangle^2 \quad (4)$$

Occasionally, these two definitions have been presented as distinct measures that happen to behave similarly in practice [3, 95]. Expressing the scalar product as  $\langle \mathbf{T}^{(1)}, \mathbf{T}^{(2)} \rangle = \text{tr}(\mathbf{T}^{(1)\text{T}} \mathbf{T}^{(2)})$  (where  $\mathbf{T}^{(1)\text{T}}$  is the transpose of  $\mathbf{T}^{(1)}$  and  $\text{tr}(\cdot)$  denotes matrix trace) and writing  $\mathbf{T}$  in terms of its spectral decomposition ( $\mathbf{T} = \mathbf{E} \mathbf{\Lambda} \mathbf{E}^{\text{T}}$ ) allows us to verify that they are, in fact, mathematically equivalent [55].

Based on the interpretation of diffusion tensors as the covariance matrix of a multivariate Gaussian distribution, Wang and Vemuri [126] propose to treat diffusion tensor fields as fields of Gaussian probability distribution functions (PDFs), and to consider the square root of the J-divergence, an information theoretical distance measure between PDFs. It is given as

$$d_J(\mathbf{T}^{(1)}, \mathbf{T}^{(2)}) = \frac{1}{2} \sqrt{\text{tr}(\mathbf{T}^{(1)-1} \mathbf{T}^{(2)} + \mathbf{T}^{(2)-1} \mathbf{T}^{(1)})} - 6 \quad (5)$$

where  $\mathbf{T}^{(1)-1}$  denotes the inverse of  $\mathbf{T}^{(1)}$ . Unlike  $d_E$ ,  $d_J$  is not a metric, since it does not fulfill the triangle inequality. A proper Riemannian metric  $d_R$  on the set of positive definite tensors that shares some of the properties of  $d_J$  is presented by Batchelor et al. [12]:

$$d_R(\mathbf{T}^{(1)}, \mathbf{T}^{(2)}) = \sqrt{\text{tr}(\log^2(\mathbf{T}^{(1)-1/2} \mathbf{T}^{(2)} \mathbf{T}^{(1)-1/2}))} \quad (6)$$

where the matrix logarithm  $\log(\cdot)$  is evaluated on the eigenvalues. Lenglet et al. adapt the idea of interpreting diffusion tensors via the corresponding Gaussian PDFs and initially employ  $d_J$  [69]. In a follow-up work [70], they use  $d_R$  and show that it can be derived from the Fisher information matrix.

The choice of metric can have significant impact on the computational efficiency of a segmentation model. In part, this is due to the fact that Equations (5) and (6) involve operations like matrix inverse and logarithm. In addition, many segmentation methods repeatedly compute tensor means, and the definition of a mean  $\mu$  changes with the chosen metric (cf. Figure 4). When using the Euclidean norm  $d_E$ , the mean can be taken component-wise, but its computation becomes more complex for  $d_J$ , and when more than two tensors are involved, it does not even have a closed form solution in case of  $d_R$  [12, 70]. In order to reduce this computational burden, Arsigny et al. [5] propose the Log-Euclidean distance  $d_L$ ; it corresponds to applying  $d_E$  after taking the matrix logarithm:

$$d_L(\mathbf{T}^{(1)}, \mathbf{T}^{(2)}) = d_E(\log(\mathbf{T}^{(1)}), \log(\mathbf{T}^{(2)})) \quad (7)$$

For many practical purposes,  $d_L$  has similar properties as  $d_J$  and  $d_R$ : Weldeselassie and Hamarneh [130] find that within their segmentation framework,  $d_L$  to  $d_J$  produce comparable

results. From a theoretical standpoint,  $d_J$  and  $d_R$  are both affine invariant: For any invertible matrix  $\mathbf{A}$ ,  $d_{\{J,R\}}(\mathbf{T}^{(1)}, \mathbf{T}^{(2)}) = d_{\{J,R\}}(\mathbf{A}\mathbf{T}^{(1)}\mathbf{A}^T, \mathbf{A}\mathbf{T}^{(2)}\mathbf{A}^T)$ .  $d_L$  is not affine invariant, but retains, among others, invariance under rotation and scaling [5]. Additionally,  $d_R$  and  $d_L$  are invariant under inversion,  $d_{\{R,L\}}(\mathbf{T}^{(1)}, \mathbf{T}^{(2)}) = d_{\{R,L\}}(\mathbf{T}^{(1)-1}, \mathbf{T}^{(2)-1})$ .

Which of these invariances are actually desirable for diffusion tensor processing is a topic of current scientific debate. Affine invariant and Log-Euclidean metrics put positive definite tensors at an infinite distance from tensors with non-positive eigenvalues. Arsigny et al. [5] argue that this is beneficial, since diffusivities should not be negative. When interpolating tensors with the Euclidean metric, the determinant of the interpolant can become larger than the determinants of the original tensors. Arsigny et al. call this effect “tensor swelling” and consider it a major problem, which is avoided by the use of their Log-Euclidean metric.

On the other hand, Pasternak et al. [94] have pointed out that while diffusivity as a physical quantity is indeed non-negative, noise and artifacts can still cause *measurements* of diffusivity to become negative. When performing statistical analysis on such measurements, replacing individual negative values with zero or a small positive value will bias the resulting estimates. More generally, they consider affine invariance to be undesirable, since diffusivity has a meaningful scale, so it makes sense to measure absolute differences (as done by  $d_E$ ), whereas affine invariant metrics effectively compute ratios. Finally, they argue that unless very specific assumptions can be made on the variability underlying the data, it is more appropriate to preserve tensor trace during interpolation (again done by  $d_E$ ) than to preserve the determinant (as done by  $d_L$ ).

Other frameworks for tensor interpolation and distance measurement have monotonically interpolated eigenvalues [76] or invariants such as fractional anisotropy [60]. However, they do not lead to closed-form distance measures, and have so far not been used for segmentation.

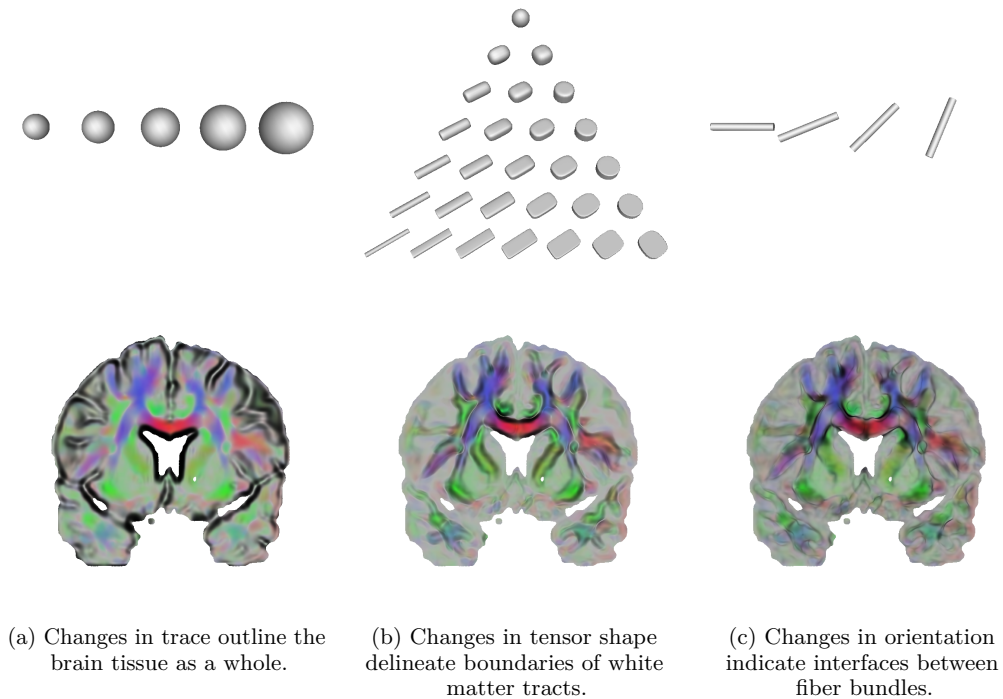
There is evidence that for DT-MRI segmentation, no unique “correct” or “best” distance measure exists. In [53] and [55], Jonasson et al. segment two different anatomical structures and point out that different distance measures gave the best results in these two cases. Similarly, Ziyang et al. [145] find that when segmenting the thalamic nuclei, concentrating on differences in principal eigenvector directions produces better results than using the full tensor information. Schultz et al. [106] demonstrate that, starting from the same initialization, an edge-based level set method will either segment the ventricle or the corpus callosum, depending on the chosen distance measure. Consequently, they propose a flexible framework in which physically meaningful user-defined weights allow the expert to customize the distance measure for specific segmentation problems.

### 3.2 Edges in Diffusion Tensor Fields

Edges are rapid changes in the data and often indicate meaningful structural boundaries. In grayscale images, edges correspond to variations in intensity, and the gradient vector indicates their direction and magnitude. In DT-MRI fields, they have a more complex structure: Gradients are third-order tensors, and the six degrees of freedom in second-order tensors lead to different types of edges, related to changes in trace, shape, or orientation (cf. Figure 5).

The first edge maps of DT-MRI data were created by Pajevic et al. [91], who distinguish two types of edges by either considering gradients in the full tensor field or only in its deviatoric (trace-free) part. Alternatively, O’Donnell et al. [85] employ normalized convolution to reduce the effect of tensor trace on the overall edge strength.

Kindlmann et al. [59] have presented a framework which decomposes the tensor field gradient into six physically meaningful edge types that cover all degrees of freedom present in the data. This is achieved by considering the gradients of tensor invariants, i.e., changes in



■ **Figure 5** Different types of edges exist in diffusion tensor fields. On the top, variations in specific tensor attributes are illustrated. On the bottom, corresponding edge maps are overlaid on slices in standard XYZ-RGB color coding.

tensor value that are associated with changes in scalar measures such as trace or fractional anisotropy. Three scalar measures are used that parameterize the full space of tensor shapes and whose gradients are orthogonal [37]. In order to capture changes in tensor orientation, the framework is supplemented with rotation tangents, describing the effect of infinitesimal rotations around the eigenvectors. Taken together, normalized invariant gradients and rotation tangents form a local basis of the space of symmetric  $3 \times 3$  matrices, and different edge types are distinguished by expressing the tensor field gradient in that basis. In a follow-up work, Schultz and Seidel [109] clarified the relation between invariant gradients and perturbation theory and demonstrate how to find analytical edge maps of anisotropy measures that are defined in terms of sorted eigenvalues, such as  $c_l$ ,  $c_p$ , and  $c_s$  [131].

Edges are low-level features; by themselves, they have not found extensive use for visualization or quantitative analysis. However, they provide guidance for some of the segmentation approaches that will be discussed in the remainder of this section [38, 106, 110]. They are also used to define higher-level features which do not imply a partitioning of the field, like interfaces between adjacent tracts [59]. Crease surfaces can be used to obtain explicit geometric representations of such features, and will be covered in Section 5.

### 3.3 Fiber Tract Segmentation

Contributions on white matter segmentation can be compared along various axes. In this section, we will consider segmentation goals and discuss different segmentation strategies and region models. Most existing approaches are based on the diffusion tensor model, but some [41, 77, 54, 127, 102, 32] have used HARDI data.

Initial works on diffusion MRI segmentation have aimed at delineating the white matter as a whole [144, 38]. However, such segmentations are already afforded by simpler acquisition schemes, such as T1-weighted imaging [27]. Segmentation tasks that explicitly rely on the contrast provided by diffusion MRI include specific structures within the white matter. The corpus callosum is the largest white matter structure in the human brain, connecting the two hemispheres, and has been a very common target of segmentation efforts [100, 70, 106, 54, 29, 130, 127, 102, 32]. Some authors have also aimed at segmenting the cortico-spinal tract [53, 41, 54, 102, 32] and several smaller structures, including (parts of) the cingulum bundles [41, 6, 127], the inferior long association bundles [53] and tracts in the brainstem [41]. Moreover, rat brain and spinal cord [126, 77, 7] as well as a phantom from excised rat spinal cords [18, 70, 32] have been the objects of investigation.

Level set methods [113, 88] have been the most frequent framework for DW-MRI segmentation. They represent the segmented boundary as the zero isocontour of a scalar field and evolve it under some partial differential equation. Zhukov et al. [144] present the earliest level set method for DT-MRI segmentation, but only make use of two derived scalar fields, which limits their method to finding the ventricles and the white matter as a whole. Most later works exploit the full tensor information: Feddern et al. [38, 39] and Schultz et al. [106] use edge-based active contours [19, 57], while most others rely on region models. For example, Wang and Vemuri [125] use a piecewise constant model [20]; Rousson et al. [100] employ multivariate Gaussian modeling of the regions, similar to [99].

As alternatives to level sets, Markov random fields [77, 6, 7] and graph-based methods [130, 127] have been used. Markov random fields [71] are based on a statistical image model. Given the observed image and optional priors, they estimate model parameters that determine a per-region distribution of image values and the per-voxel region membership in a Bayesian framework. Graph-based methods [129, 66] have already been mentioned in Section 2.2: They treat each voxel as a node in a graph, and assign edge weights based on similarity in diffusion properties and spatial proximity. Fiber tract segmentation was also approached with traditional visualization tools by Schultz et al. [110]: They extract isosurfaces that outline the white matter core and use a watershed-type mesh segmentation to identify individual bundles, combining edge- with region-based information.

The simplest models used for segmentation assume a constant diffusion tensor per region, or a Gaussian distribution of tensors. In the presence of bending fibers, such assumptions are problematic, since the mean tensor tends to become isotropic and the model can lose its discriminative power. This problem has been addressed in the following ways: Wang and Vemuri [126] replace their original piecewise constant by a piecewise smooth model [84]. De Luis-García and Alberola-López [29] employ a mixture of Gaussians. Finally, Awate et al. [6] present a fuzzy segmentation framework that is based on nonparametric region models.

Methodically, “fast-marching” [93] or “flow-based” [18] tractography lies in between streamline-based tractography and white matter segmentation. It starts with a level set representation of a small sphere, initialized at some user-specified seed. The initial surface is propagated in normal direction with a speed that depends on the estimated likelihood of a fiber connection in the given direction. Each voxel records the time at which it was first reached by the surface; a gradient descent in the resulting time-of-arrival map connects any point in the domain to the original seed, and assigns a likelihood to those paths, making a connection to probabilistic tractography.

On the other hand, Jonasson et al. [53] define propagation speed based on the local similarity of diffusion properties, stop surface evolution when the speed drops below some threshold, and interpret the final surface as the outline of a fiber bundle, which makes a

connection to traditional edge-based segmentation schemes. Conceptually, this strategy corresponds to region growing with curvature-based regularization. Savadjiev et al. [102] use a simpler, unregularized region growing scheme, but derive a similarity measure from the differential geometry of local streamline neighborhoods rather than diffusion properties.

For segmentation of HARDI data, Jonasson et al. [54] transform three-dimensional fields of orientation distribution functions (ODFs) to a five-dimensional scalar field, which they segment with a hypersurface. Hagmann et al. [41] rely on the same five-dimensional position-orientation space, but employ a Markov random field rather than a level set method for the segmentation. Similarly, McGraw et al. [77] use a hidden Markov measure field, but model the ODFs as mixtures of von Mises-Fisher distributions. Finally, Descoteaux and Deriche [32] model the ODFs with spherical harmonics and apply the single-Gaussian region model by Rousson et al. [100] to the resulting coefficients.

### 3.4 Gray Matter Segmentation

Finding the major nuclei of the thalamus has been the first example of gray matter segmentation based on DW-MRI. The reason for this is that the thalamus contains homogeneously oriented axons (“striations”) that provide contrast in diffusion imaging.

Wiegell et al. [133] combine diffusion tensor dissimilarity and spatial distance to cluster voxels inside of the thalamus via a k-means algorithm. To obtain improved results, other authors employed normalized graph cuts [145], level sets [55], and the mean shift algorithm [34]. To avoid having to determine correspondences explicitly when comparing the segmentation results on different subjects, Ziyang and Westin [146] segment all datasets jointly.

A conceptually different approach to segmenting the thalamus goes back to Behrens et al. [14], who map manually defined cortex areas to the thalamus via a probabilistic tracking of the cortico-thalamic connections. In a follow-up, Johansen-Berg et al. [52] validate this method by comparing the cortex areas that are reached by a tractography from the centers of thalamic activations as determined by functional MRI.

Johansen-Berg et al. [51] and Anwender et al. [4] demonstrate that clustering results from probabilistic tractography allows one to segment certain parts of the cortex into functionally distinct regions. This observation is exploited by Schultz et al. [111] in their definition of topological features in diffusion MRI data, which will be detailed in the next section.

## 4 Topological Methods

In the feature-based visualization of flow fields, topological methods are a well-established approach. Introduced to visualization by Helman and Hesselink [44], they have been researched widely since then [119, 103, 128]. Topological methods extract qualitative structures from the data by considering the asymptotic behavior of streamlines, effectively partitioning the domain into regions in which all streamlines start in the same source and end in the same sink. The interfaces between these regions constitute the topological skeleton, a concise description of the data which is invariant over all structurally equivalent fields.

The eigenvector fields derived from a symmetric second-order tensor field differ from proper vector fields in the fact that they lack orientation. Delmarcelle and Hesselink [31] have demonstrated how the basic definitions of vector field topology can be transferred to eigenvectors. In a follow-up work, Hesselink et al. [45] also considered three-dimensional tensor fields. Points at which two or more eigenvalues coincide are the fundamental features in tensor topology, and later works [28, 142] have clarified the fact that in generic 3D data, these “degenerate” loci form stable lines.

Even though it had previously been proposed to apply tensor topology to diffusion tensor fields [143], Schultz et al. [111] were the first to publish results on this type of data. Experimenting with the algorithm by Zheng et al. [142], they found that the utility of tensor topology on data from brain diffusion MRI is limited by the facts that the features do not have a clear correlation to anatomical structures, and that they are very sensitive to measurement noise and the choice of interpolation. This observation is partly explained by the fact that standard single fiber models predict diffusion tensors with two equal eigenvalues. On idealized diffusion tensor fields, this imposes a constraint which violates the genericity assumption on which tensor topology is founded.

In order to transfer the basic idea of topological visualization to diffusion MRI, Schultz et al. [111] instead consider the asymptotic behavior of a probabilistic fiber tracking algorithm and identify fuzzy subvolumes which are likely to connect functionally distinct regions of the brain. By rendering semi-transparent confidence hulls around the core structures, the uncertainty in the feature boundaries is conveyed visually.

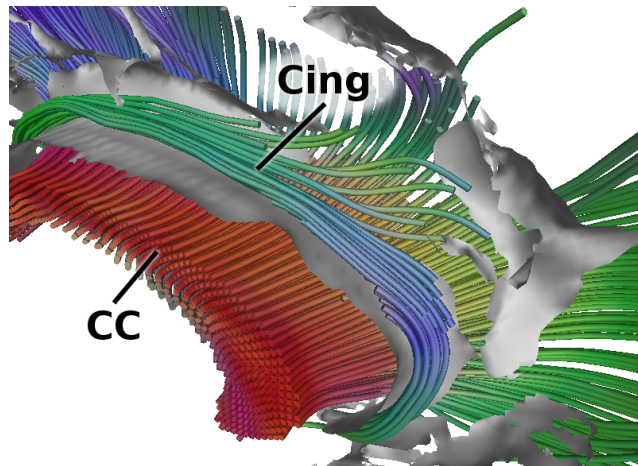
Inspired by Lagrangian coherent structures [42], Hlawitschka et al. [46] present a framework that visually highlights boundaries along which the streamlines from nearby seeds diverge notably after a fixed and finite integration time. Even though they are not the result of an asymptotic analysis, such boundaries are similar to the topological skeleton in that they separate regions of different qualitative streamline behavior. Finally, it has been pointed out by Salzbrunn and Scheuermann [101] that streamline clustering (cf. Section 2) can be considered as an alternative generalization of vector field topology, in particular when the similarity measure is based on the endpoints, as in [17].

## 5 Anisotropy Crease Surfaces and Lines

In typical scalar fields, local maxima and minima form isolated points. Creases generalize these extrema to higher-dimensional structures, like extremal lines and surfaces. Ridges generalize local maxima, while valleys correspond to local minima. Even though the most adequate crease definition is not undisputed [64], the so-called “height crease definition” [43] has become a well-researched tool to find medial axes in grayscale images [96] and has been extended towards applications as diverse as medical image analysis, molecular modeling, and analysis of fluid flows [35].

In the context of DW-MRI, ridge surfaces and lines were used in order to obtain reliable spatial statistics in group studies. To localize variations in fractional anisotropy (FA) between two groups (typically, patients vs. healthy controls), many previous studies would register individual datasets to a volumetric template and subsequently perform a local statistical analysis, effectively comparing anisotropy values in individual voxels over all subjects. The reliability of such voxel-based methods is limited by inevitable inaccuracies in registration, varying degrees of partial voluming, and heuristic choices of the smoothing kernel. To ameliorate these problems, Smith et al. [117] extract ridges in a group-averaged FA map. In each individual dataset, locally maximal values of FA are then projected onto the common ridge and statistical tests are done on the ridge manifold. This projection compensates slight misalignments and does not involve any smoothing of the modeled data, leading to more objective and valid results.

The algorithm by Smith et al. [117] employs a thinning technique to produce a binary mask, indicating which voxels are part of the ridge. In contrast, Kindlmann et al. [62] use the height crease definition along with analytical derivatives of FA to extract a high-resolution triangle mesh representation of ridge and valley surfaces, which they name “anisotropy



■ **Figure 6** A valley surface in fractional anisotropy (gray) separates the right cingulum bundle (Cing) from the corpus callosum (CC).

creases” (cf. Figure 6). In a follow-up to this work, Schultz et al. [112] present an improved algorithm that captures the surface boundaries more precisely and is approximately one order of magnitude faster on typical DT-MRI data. Some white matter structures, including parts of the cingulum bundles, are tube-like rather than sheet-like, so their cores are better described by lines than by surfaces. In this respect, the algorithm to extract FA ridge lines presented by Tricoche et al. [120] complements the original method from [62].

Intuitively, creases are similar to topological methods as surveyed in Section 4 in that they reduce the dataset to a structural skeleton. More formally, Tricoche et al. [120] point out that degenerate lines in tensor topology are a subset of the crease lines in a tensor invariant called mode, which captures the transition between linear and planar anisotropy. In this sense, anisotropy creases remedy the shortcomings of tensor topology in DT-MRI data by replacing mode with FA, an invariant which is more widely used for anatomical analysis and less affected by noise. A second link between both methods has been found by Schultz et al. [112]. In their theoretical analysis of crease surface topology, they observe that degenerate lines in the Hessians of the considered anisotropy measure (rather than in the diffusion tensor field itself) form one type of crease surface boundary, and they employ the gradient descent proposed by Zheng et al. [142] to localize it.

Since measurement noise and fine-scale structures induce spurious local extrema, extraction of stable and expressive creases typically requires some amount of filtering. While Smith et al. [117] process group mean images which are smoothed implicitly by the involved averaging, Kindlmann et al. [62] work on individual datasets and thus have to perform explicit filtering. However, the adequate smoothing extent is not known a priori and can even vary spatially, because anatomical structures differ in size. In computer vision, this problem has been addressed by treating the amount of smoothing as a free parameter, and analyzing the family of images generated by all possible values along this additional “scale” axis [72]. A particle-based approach to extract creases of variable dimensionality from scale space has been presented by Kindlmann et al. [61].

Extracting anisotropy creases and finding medial structures from fiber bundles (Section 2.5) can be considered as competing approaches to defining a white matter skeleton. This becomes especially clear in a work by Yushkevich et al. [137]: By fitting medial surface models to fiber bundles, they generate surfaces that lend themselves to a similar local statistical analysis as

it was done by Smith et al. [117]. Ultimately, the choice between both options might depend on the exact goals of a study: An analysis based on streamline clusters is more specific to individual tracts, but relies on a correct clustering (in [137], this step is performed by an expert). Anisotropy creases are less specific, but require less manual intervention and make it easier to cover the whole white matter.

In the visualization community, crease manifolds were not only treated as a tool for quantitative analysis: Schultz et al. [112] found that DT-MRI streamsurfaces, which had been proposed previously to illustrate regions of planar diffusion [139], are ill-defined in typical data, and demonstrate that planarity ridge surfaces can replace them.

## 6 Conclusion and Future Directions

One of the challenges in the visualization of DW-MRI data is the high information density: Diffusion tensor MRI produces symmetric second-order tensors with six degrees of freedom per voxel, HARDI models have an even larger number of parameters. Feature extraction is an established strategy to provide a layer of abstraction that allows for visual inspection of such complex data, while preserving information that is relevant to a given application.

In this paper, we have summarized the state of the art in feature-based DW-MRI visualization. Even though different communities have contributed to this field, we were able to highlight a number of close links between the presented approaches. Most prominently, a recurrent theme in streamline clustering (Section 2), white matter segmentation (Section 3), and fuzzy diffusion MRI topology (Section 4) is to identify the spatial extent of anatomically relevant fiber bundles.

DW-MRI visualization is a relatively young field. Consequently, much of the initial work has concentrated on brainstorming new ideas, and many methods have been proposed without a systematic comparison to the state of the art. As the field matures, one important aspect of future research will be to clarify the relation between existing techniques in a more formal manner. Ideally, the community should agree on quantitative benchmarks that help to ensure that we are not only creating more, but actually better ways of analyzing DW-MRI data. This would be greatly facilitated by a public library of datasets, along with atlases that provide ground truth for segmentation and fiber clustering. For grayscale and color images, such libraries exist and are actively used in the computer vision community [75]. Even though some diffusion-based white matter atlases are available on the web,<sup>1</sup> we are not aware of any works that have used them for validation.

When research on DW-MRI visualization was still in its infancy, flow visualization already offered an impressive variety of feature-based techniques [97]. Consequently, many methods for vector fields have been transferred to tensor fields and applied to DT-MRI data. With time, this relation should become more reciprocal: For example, the uncertainty in connections inferred from DW-MRI inspired a fuzzy topological visualization [111] before the topology of uncertain vector fields had been considered [89]. In the relation between flow and diffusion visualization, it is important to remember that despite the many analogies, flow and diffusion are physically different processes. Flow is described by the Navier-Stokes equations, while diffusion is governed by Fick's laws [40]. One important consequence of this fact is that flow has a direction, while the displacement probabilities of free diffusion exhibit antipodal

---

<sup>1</sup> This includes an atlas available from the Laboratory of Neuro Imaging at UCLA (<http://www.loni.ucla.edu/Atlases/>) and two atlases from John Hopkins University, included in the FM-RIB Software Library provided by Oxford University (<http://www.fmrib.ox.ac.uk/fsl/fslview/atlas-descriptions.html>).

symmetry. The hindered diffusion processes typically met in biological tissue are even more complex and still not fully understood [13].

With respect to the development of new methods, future challenges of the field include:

- *Adapt methods to HARDI.* While high-angular resolution imaging has been a very active topic in neuroimaging for several years, the visualization community has started to investigate it only recently [47, 108]. Feature extraction is even more important for this more complex type of data than it is for DT-MRI. For example, Jonasson et al. [56] point out that streamline clustering becomes essential to disentangle intersecting fiber tracts reconstructed via HARDI.
- *Reproducibility and feature matching* over different subjects have to be achieved before methods can be used in neuroscience or medical studies, but are considered only rarely in the context of visualization (e.g., [80, 138]). Moreover, *statistical methods* and the *quantification of uncertainty and variance* still receive too little attention in the visualization literature.
- A closely related task is to *make existing methods more stable*. One example of this is the concept of scale space, which facilitates feature detection under noise and varying scales. For 2D images, scale space is well-established in image processing and computer vision. However, it has started to find its way into the visualization of large 3D datasets only recently [61].
- Even though we believe that there is legitimate fundamental research to be done in visualization, we should keep an eye on the fact that the ultimate goal of our efforts is to *facilitate new insights*. This can be achieved by using visualization to support generation of new hypotheses, as part of a framework that enables quantitative analysis and hypothesis testing, or as a debugging tool for the scientific workflow.

**Acknowledgement** I would like to thank Gordon Kindlmann for helpful discussions about this paper, and Alfred Anwander (MPI CBS, Leipzig, Germany) for providing the DW-MRI dataset that was used to create some of the figures.

---

## References

- 1 D. Akers. CINCH: a cooperatively designed marking interface for 3D pathway selection. In *Proc. ACM UIST*, pages 33–42, 2006.
- 2 D. C. Alexander. An introduction to computational diffusion MRI: The diffusion tensor and beyond. In J. Weickert and H. Hagen, editors, *Visualization and Processing of Tensor Fields*, pages 83–106. Springer, 2006.
- 3 D. C. Alexander, J. C. Gee, and R. Bajcsy. Similarity measures for matching diffusion tensor images. In T. P. Pridmore and D. Elliman, editors, *Proceedings of the British Machine Vision Conference*, pages 93–102, Nottingham, September 1999.
- 4 A. Anwander, M. Tittgemeyer, D. von Cramon, A. Friederici, and T. Knösche. Connectivity-based parcellation of broca’s area. *Cerebral Cortex*, 17(4):816–825, 2007.
- 5 V. Arsigny, P. Fillard, X. Pennec, and N. Ayache. Log-euclidean metrics for fast and simple calculus on diffusion tensors. *Magnetic Resonance in Medicine*, 56(2):411–421, 2006.
- 6 S. P. Awate, H. Zhang, and J. C. Gee. A fuzzy, nonparametric segmentation framework for DTI and MRI analysis: With applications to DTI-tract extraction. *IEEE Transactions on Medical Imaging*, 26(11):1525–1536, 2007.
- 7 A. Barmpoutis, B. C. Vemuri, T. M. Shepherd, and J. R. Forder. Tensor splines for interpolation and approximation of DT-MRI with applications to segmentation of isolated rat hippocampi. *IEEE Transactions on Medical Imaging*, 26(11):1537–1546, 2007.

- 8 P. J. Basser and D. K. Jones. Diffusion-tensor MRI: theory, experimental design and data analysis – a technical review. *NMR in Biomedicine*, 15(7–8):456–467, 2002.
- 9 P. J. Basser, J. Mattiello, and D. L. Bihan. Estimation of the effective self-diffusion tensor from the NMR spin echo. *Journal of Magnetic Resonance*, B(103):247–254, 1994.
- 10 P. J. Basser, S. Pajevic, C. Pierpaoli, J. Duda, and A. Aldroubi. In vivo fiber tractography using DT-MRI data. *Magnetic Resonance in Medicine*, 44:625–632, 2000.
- 11 P. G. Batchelor, F. Calamante, J.-D. Tournier, D. Atkinson, D. L. G. Hill, and A. Connelly. Quantification of the shape of fiber tracts. *Magnetic Resonance in Medicine*, 55:894–903, 2006.
- 12 P. G. Batchelor, M. Moakher, D. Atkinson, F. Calamante, and A. Connelly. A rigorous framework for diffusion tensor calculus. *Magnetic Resonance in Medicine*, 53:221–225, 2005.
- 13 C. Beaulieu. The basis of anisotropic water diffusion in the nervous system – a technical review. *NMR in Biomedicine*, 15(7–8):435–455, 2002.
- 14 T. E. J. Behrens, H. Johansen-Berg, M. W. Woolrich, S. M. Smith, C. A. M. Wheeler-Kingshott, P. A. Boulby, G. J. Barker, E. L. Sillery, K. Sheehan, O. Ciccarelli, A. J. Thompson, J. M. Brady, and P. M. Matthews. Non-invasive mapping of connections between human thalamus and cortex using diffusion imaging. *Nature Neuroscience*, 6(7):750–757, 2003.
- 15 J. Blaas, C. P. Botha, B. Peters, F. M. Vos, and F. H. Post. Fast and reproducible fiber bundle selection in DTI visualization. In C. Silva, E. Gröller, and H. Rushmeier, editors, *Proc. IEEE Visualization 2005*, pages 59–64, 2005.
- 16 A. Brun, H. Knutsson, H. J. Park, M. E. Shenton, and C.-F. Westin. Clustering fiber tracts using normalized cuts. In C. Barillot, D. Haynor, and P. Hellier, editors, *Proc. Medical Image Computing and Computer-Assisted Intervention (MICCAI)*, volume 3216 of *LNCS*, pages 368–375. Springer, 2004.
- 17 A. Brun, H.-J. Park, H. Knutsson, and C.-F. Westin. Coloring of DT-MRI fiber traces using laplacian eigenmaps. In R. Moreno-Díaz and F. Pichler, editors, *Proc. Computer Aided Systems Theory (EUROCAST)*, volume 2809 of *LNCS*, pages 518–529. Springer, 2003.
- 18 J. S. W. Campbell, K. Siddiqi, V. V. Rymar, A. F. Sadikot, and G. B. Pike. Flow-based fiber tracking with diffusion tensor and q-ball data: Validation and comparison to principal diffusion direction techniques. *NeuroImage*, 27:725–736, 2005.
- 19 V. Caselles, R. Kimmel, and G. Sapiro. Geodesic active contours. In *Proc. International Conference on Computer Vision (ICCV)*, pages 694–699, 1995.
- 20 T. F. Chan and L. A. Vese. Active contours without edges. *IEEE Transactions on Image Processing*, 10(2):266–277, 2001.
- 21 W. Chen, Z. Ding, S. Zhang, A. MacKay-Brandt, S. Correia, H. Qu, J. A. Crow, D. F. Tate, Z. Yan, and Q. Peng. A novel interface for interactive exploration of DTI fibers. *IEEE Transactions on Visualization and Computer Graphics*, 15(6):1433–1440, 2009.
- 22 W. Chen, S. Zhang, S. Correia, and D. S. Ebert. Abstractive representation and exploration of hierarchically clustered diffusion tensor fiber tracts. *Computer Graphics Forum (Proc. EuroVis)*, 27(3):1071–1078, 2008.
- 23 T. E. Conturo, N. F. Lori, T. S. Cull, E. Akbudak, A. Z. Snyder, J. S. Shimony, R. C. McKinstry, H. Burton, and M. E. Raichle. Tracking neuronal fiber pathways in the living human brain. *Proc. Natl. Acad. Sci. USA*, 96:10422–10427, 1999.
- 24 I. Corouge, P. T. Fletcher, S. Joshi, S. Gouttard, and G. Gerig. Fiber tract-oriented statistics for quantitative diffusion tensor MRI analysis. *Medical Image Analysis*, 10:786–798, 2006.
- 25 I. Corouge, S. Gouttard, and G. Gerig. A statistical shape model of individual fiber tracts extracted from diffusion tensor MRI. In C. Barillot, D. R. Haynor, and P. Hellier, editors,

- Proc. Medical Image Computing and Computer-Assisted Intervention (MICCAI)*, volume 3217 of *LNCS*, pages 671–679. Springer, 2004.
- 26 I. Corouge, S. Gouttard, and G. Gerig. Towards a shape model of white matter fiber bundles using diffusion tensor MRI. In *Proc. IEEE International Symposium on Biomedical Imaging (ISBI)*, pages 344–347, 2004.
  - 27 M. B. Cuadra, L. Cammoun, T. Butz, O. Cuisenaire, and J.-P. Thiran. Comparison and validation of tissue modelization and statistical classification methods in t1-weighted MR brain images. *IEEE Transactions on Medical Imaging*, 24(12):1548–1565, 2005.
  - 28 J. Damon. Generic structure of two-dimensional images under gaussian blurring. *SIAM Journal on Applied Mathematics*, 59(1):97–138, 1998.
  - 29 R. de Luis-García and C. Alberola-López. Mixtures of gaussians on tensor fields for DT-MRI segmentation. In N. Ayache, S. Ourselin, and A. Maeder, editors, *Proc. Medical Image Computing and Computer-Assisted Intervention (MICCAI)*, volume 4791 of *LNCS*, pages 319–326. Springer, 2007.
  - 30 T. Delmarcelle and L. Hesselink. Visualizing second-order tensor fields with hyperstreamlines. *IEEE Computer Graphics and Applications*, 13(4):25–33, 1993.
  - 31 T. Delmarcelle and L. Hesselink. The topology of symmetric, second-order tensor fields. In R. D. Bergeron and A. E. Kaufman, editors, *Proc. IEEE Visualization*, pages 140–147, 1994.
  - 32 M. Descoteaux and R. Deriche. High angular resolution diffusion MRI segmentation using region-based statistical surface evolution. *Journal of Mathematical Imaging and Vision*, 33(2):239–252, 2009.
  - 33 Z. Ding, J. C. Gore, and A. W. Anderson. Classification and quantification of neuronal fiber pathways using diffusion tensor MRI. *Magnetic Resonance in Medicine*, 49:716–721, 2003.
  - 34 Y. Duan, X. Li, and Y. Xi. Thalamus segmentation from diffusion tensor magnetic resonance imaging. *International Journal of Biomedical Imaging*, 2007, 2007.
  - 35 D. Eberly. *Ridges in Image and Data Analysis*, volume 7 of *Computational Imaging and Vision*. Kluwer Academic Publishers, 1996.
  - 36 F. Enders, N. Sauber, D. Merhof, P. Hastreiter, C. Nimsky, and M. Stamminger. Visualization of white matter tracts with wrapped streamlines. In C. Silva, E. Gröller, and H. Rushmeier, editors, *Proc. IEEE Visualization*, pages 51–58, 2005.
  - 37 D. B. Ennis and G. Kindlmann. Orthogonal tensor invariants and the analysis of diffusion tensor magnetic resonance images. *Magnetic Resonance in Medicine*, 55(1):136–146, 2006.
  - 38 C. Feddern, J. Weickert, and B. Burgeth. Level-set methods for tensor-valued images. In O. D. Faugeras and N. Paragios, editors, *Proc. IEEE Workshop on Geometric and Level Set Methods in Computer Vision*, pages 65–72, 2003.
  - 39 C. Feddern, J. Weickert, B. Burgeth, and M. Welk. Curvature-driven PDE methods for matrix-valued images. *International Journal of Computer Vision*, 69(1):93–107, 2006.
  - 40 A. Fick. Über Diffusion. *Annalen der Physik*, 170(1):59–86, 1855.
  - 41 P. Hagmann, L. Jonasson, T. Deffieux, R. Meuli, J.-P. Thiran, and V. J. Wedeen. Fibertract segmentation in position orientation space from high angular resolution diffusion MRI. *NeuroImage*, 32(2):665–675, 2006.
  - 42 G. Haller. Distinguished material surfaces and coherent structures in three-dimensional fluid flows. *Physica D*, 149:248–277, 2001.
  - 43 R. M. Haralick. Ridges and valleys on digital images. *Computer Vision, Graphics, and Image Processing*, 22:28–38, 1983.
  - 44 J. Helman and L. Hesselink. Representation and display of vector field topology in fluid flow data sets. *Computer*, 22(8):27–36, 1989.

- 45 L. Hesselink, Y. Levy, and Y. Lavin. The topology of symmetric, second-order 3D tensor fields. *IEEE Transactions on Visualization and Computer Graphics*, 3(1):1–11, 1997.
- 46 M. Hlawitschka, C. Garth, X. Tricoche, G. Kindlmann, G. Scheuermann, K. I. Joy, and B. Hamann. Direct visualization of fiber information by coherence. *International Journal of Computer Assisted Radiology and Surgery*, 5(2):125–131, 2010.
- 47 M. Hlawitschka and G. Scheuermann. HOT-lines: Tracking lines in higher order tensor fields. In C. Silva, E. Gröller, and H. Rushmeier, editors, *Proc. IEEE Visualization*, pages 27–34, 2005.
- 48 M. A. Horsfield and D. K. Jones. Applications of diffusion-weighted and diffusion tensor MRI to white matter diseases – a review. *NMR in Biomedicine*, 15(7–8):570–577, 2002.
- 49 E. Hsu. Generalized line integral convolution rendering of diffusion tensor fields. In *Proc. International Society of Magnetic Resonance in Medicine (ISMRM)*, page 790, 2001.
- 50 R. Jianu, Ç. Demiralp, and D. H. Laidlaw. Exploring 3D DTI fiber tracts with linked 2D representations. *IEEE Transactions on Visualization and Computer Graphics*, 15(6):1449–1456, 2009.
- 51 H. Johansen-Berg, T. Behrens, M. Robson, I. Drobnjak, M. Rushworth, J. Brady, S. Smith, D. Higham, and P. Matthews. Changes in connectivity profiles define functionally distinct regions in human medial frontal cortex. *Proc. National Academy of Sciences of the United States of America (PNAS)*, 101(36):13335–13340, 2004.
- 52 H. Johansen-Berg, T. E. J. Behrens, E. Sillery, O. Ciccarelli, A. J. Thompson, S. M. Smith, and P. M. Matthews. Functional-anatomical validation and individual variation of diffusion tractography-based segmentation of the human thalamus. *Cerebral Cortex*, 15(1):31–39, 2005.
- 53 L. Jonasson, X. Bresson, P. Hagmann, O. Cuisenaire, R. Meuli, and J.-P. Thiran. White matter fiber tract segmentation in DT-MRI using geometric flows. *Medical Image Analysis*, 9(3):223–236, 2005.
- 54 L. Jonasson, X. Bresson, J.-P. Thiran, V. J. Wedeen, and P. Hagmann. Representing diffusion MRI in 5-D simplifies regularization and segmentation of white matter tracts. *IEEE Transactions on Medical Imaging*, 26(11):1547–1554, 2007.
- 55 L. Jonasson, P. Hagmann, C. Pollo, X. Bresson, C. R. Wilson, R. Meuli, and J.-P. Thiran. A level set method for segmentation of the thalamus and its nuclei in DT-MRI. *Signal Processing*, 87(2):309–321, 2007.
- 56 L. Jonasson, P. Hagmann, J.-P. Thiran, and V. J. Wedeen. Fiber tracts of high angular resolution diffusion MRI are easily segmented with spectral clustering. In *Proc. International Society for Magnetic Resonance in Medicine (ISMRM)*, 2005.
- 57 S. Kichenassamy, A. Kumar, P. Olver, A. Tannenbaum, and A. Yezzi. Gradient flows and geometric active contour models. In *Proc. International Conference on Computer Vision (ICCV)*, pages 810–815, 1995.
- 58 G. Kindlmann. Superquadric tensor glyphs. In *Proc. Eurographics/IEEE Symposium on Visualization (SymVis)*, pages 147–154, 2004.
- 59 G. Kindlmann, D. Ennis, R. Whitaker, and C.-F. Westin. Diffusion tensor analysis with invariant gradients and rotation tangents. *IEEE Transactions on Medical Imaging*, 26(11):1483–1499, 2007.
- 60 G. Kindlmann, R. San José Estépar, M. Niethammer, S. Haker, and C.-F. Westin. Geodesic-loxodromes for diffusion tensor interpolation and difference measurement. In N. Ayache, S. Ourselin, and A. Maeder, editors, *Proc. Medical Image Computing and Computer-Assisted Intervention (MICCAI), Part I*, volume 4791 of *LNCS*, pages 1–9. Springer, 2007.
- 61 G. Kindlmann, R. San José Estépar, S. M. Smith, and C.-F. Westin. Sampling and visualizing creases with scale-space particles. *IEEE Transactions on Visualization and Computer Graphics (Proc. IEEE Visualization)*, 15(6):1415–1424, 2009.

- 62 G. Kindlmann, X. Tricoche, and C.-F. Westin. Delineating white matter structure in diffusion tensor MRI with anisotropy creases. *Medical Image Analysis*, 11(5):492–502, 2007.
- 63 G. Kindlmann, D. Weinstein, and D. Hart. Strategies for direct volume rendering of diffusion tensor fields. *IEEE Transactions on Visualization and Computer Graphics*, 6(2):124–138, April 2000.
- 64 J. J. Koenderink and A. J. van Doorn. Local features of smooth shapes: Ridges and courses. In B. C. Vemuri, editor, *Geometric Methods in Computer Vision II*, volume 2031 of *Proc. of SPIE*, pages 2–13, 1993.
- 65 H. W. Kuhn. The hungarian method for the assignment problem. *Naval Research Logistics Quarterly*, 2:83–87, 1955.
- 66 S. Lafon and A. B. Lee. Diffusion maps and coarse-graining: A unified framework for dimensionality reduction, graph partitioning, and data set parameterization. *IEEE Transactions on Pattern Analysis and Machine Intelligence*, 28(9):1393–1403, 2006.
- 67 D. H. Laidlaw, E. T. Ahrens, D. Kremers, M. J. Avalos, R. E. Jacobs, and C. Readhead. Visualizing diffusion tensor images of the mouse spinal cord. In *Proc. IEEE Visualization*, pages 127–134, 1998.
- 68 D. Le Bihan, E. Breton, D. Lallemand, P. Grenier, E. Cabanis, and M. Laval-Jeantet. MR imaging of intravoxel incoherent motions: Application to diffusion and perfusion in neurologic disorders. *Radiology*, 161(2):401–407, 1986.
- 69 C. Lenglet, M. Rousson, and R. Deriche. Segmentation of 3D probability density fields by surface evolution: Application to diffusion MRI. In C. Barillot, D. R. Haynor, and P. Hellier, editors, *Proc. Medical Image Computing and Computer-Assisted Intervention (MICCAI)*, volume 3216 of *LNCS*, pages 18–25. Springer, 2004.
- 70 C. Lenglet, M. Rousson, and R. Deriche. DTI segmentation by statistical surface evolution. *IEEE Transactions on Medical Imaging*, 25(6):685–700, 2006.
- 71 S. Z. Li. *Markov Random Field Modeling in Image Analysis*. Advances in Pattern Recognition. Springer, 3rd edition, 2009.
- 72 T. Lindeberg. Scale-space. In B. Wah, editor, *Encyclopedia of Computer Science and Engineering*, volume IV, pages 2495–2504. Wiley, 2009.
- 73 M. Maddah, W. E. L. Grimson, S. K. Warfield, and W. M. Wells. A unified framework for clustering and quantitative analysis of white matter fiber tracts. *Medical Image Analysis*, 12:191–202, 2008.
- 74 M. Maddah, A. U. J. Mewes, S. Haker, W. E. L. Grimson, and S. K. Warfield. Automated atlas-based clustering of white matter fiber tracts from DTMRI. In J. Duncan and G. Gerig, editors, *Proc. Medical Image Computing and Computer-Assisted Intervention (MICCAI)*, volume 3749 of *LNCS*, pages 188–195. Springer, 2005.
- 75 D. Martin, C. Fowlkes, D. Tal, and J. Malik. A database of human segmented natural images and its application to evaluating segmentation algorithms and measuring ecological statistics. In *Proc. Int'l Conf. on Computer Vision (ICCV)*, volume 2, pages 416–423, 2001.
- 76 Y. Masutani, S. Aoki, Z. Liu, O. Abe, and K. Ohtomo. A hybrid tensor field interpolation approach for white matter fiber tract modeling. *Int'l J. of Computer Assisted Radiology and Surgery (Proc. CARS)*, 2(Suppl. 1):S22–S24, 2007.
- 77 T. McGraw, B. Vemuri, R. Yeziarski, and T. Mareci. Segmentation of high angular resolution diffusion MRI modeled as a field of von mises-fisher mixtures. In A. Leonardis, H. Bischof, and A. Pinz, editors, *Proc. European Conference on Computer Vision (ECCV)*, Part III, volume 3953 of *LNCS*, pages 463–475. Springer, 2006.
- 78 D. Merhof, M. Meister, E. Bingöl, P. Hastreiter, C. Nimsy, and G. Greiner. Generation of hulls encompassing neuronal pathways based on tetrahedralization and 3D alpha shapes. In A. Horsch, T. Deserno, H. Handels, H.-P. Meinzer, and T. Tolxdorff, editors, *Bildverarbeitung für die Medizin*, pages 308–312. Springer, 2007.

- 79 D. Merhof, M. Meister, E. Bingöl, C. Nimsky, and G. Greiner. Isosurface-based generation of hulls encompassing neuronal pathways. *Stereotactic and Functional Neurosurgery*, 87:50–60, 2009.
- 80 B. Moberts, A. Vilanova, and J. J. van Wijk. Evaluation of fiber clustering methods for diffusion tensor imaging. In *Proc. IEEE Visualization*, pages 65–72, 2005.
- 81 J. Modersitzki. *Numerical methods for image segmentation*. Oxford University Press, 2004.
- 82 S. Mori, B. J. Crain, V. P. Chacko, and P. C. M. van Zijl. Three-dimensional tracking of axonal projections in the brain by magnetic resonance imaging. *Annals of Neurology*, 45(2):265–269, 1999.
- 83 S. Mori and P. C. van Zijl. Fiber tracking: principles and strategies – a technical review. *NMR in Biomedicine*, 15:468–480, 2002.
- 84 D. Mumford and J. Shah. Optimal approximations by piecewise smooth functions and associated variational-problems. *Communications on Pure and Applied Mathematics*, 42(5):577–685, 1989.
- 85 L. O’Donnell, W. E. L. Grimson, and C.-F. Westin. Interface detection in diffusion tensor MRI. In C. Barillot, D. Haynor, and P. Hellier, editors, *Proc. Medical Image Computing and Computer-Assisted Intervention (MICCAI)*, volume 3216 of *LNCS*, pages 360–367. Springer, 2004.
- 86 L. O’Donnell and C.-F. Westin. Automatic tractography segmentation using a high-dimensional white matter atlas. *IEEE Transactions on Medical Imaging*, 26(11):1562–1575, 2007.
- 87 L. J. O’Donnell, C.-F. Westin, and A. J. Golby. Tract-based morphometry for white matter group analysis. *NeuroImage*, 45:832–844, 2009.
- 88 S. Osher and R. Fedkiw. *Level Set Methods and Dynamic Implicit Surfaces*. Springer, 2003.
- 89 M. Otto, T. Germer, H.-C. Hege, and H. Theisel. Uncertain 2D vector field topology. *Computer Graphics Forum (Proc. Eurographics)*, 29(2):347–356, 2010.
- 90 E. Özarslan and T. Mareci. Generalized diffusion tensor imaging and analytical relationships between diffusion tensor imaging and high angular resolution diffusion imaging. *Magnetic Resonance in Medicine*, 50:955–965, 2003.
- 91 S. Pajevic, A. Aldroubi, and P. J. Basser. A continuous tensor field approximation of discrete DT-MRI data for extracting microstructural and architectural features of tissue. *Journal of Magnetic Resonance*, 154:85–100, 2002.
- 92 S. Pajevic and C. Pierpaoli. Color schemes to represent the orientation of anisotropic tissues from diffusion tensor data: application to white matter fiber tract mapping in the human brain. *Magnetic Resonance in Medicine*, 42(3):526–540, 1999.
- 93 G. J. M. Parker, C. A. M. Wheeler-Kingshott, and G. J. Barker. Estimating distributed anatomical connectivity using fast marching methods and diffusion tensor imaging. *IEEE Transactions on Medical Imaging*, 21(5):505–512, 2002.
- 94 O. Pasternak, N. Sochen, and P. J. Basser. The effect of metric selection on the analysis of diffusion tensor MRI data. *NeuroImage*, 49:2190–2204, 2010.
- 95 T. Peeters, P. Rodrigues, A. Vilanova, and B. ter Haar Romeny. Analysis of distance/similarity measures for diffusion tensor imaging. In D. H. Laidlaw and J. Weickert, editors, *Visualization and Processing of Tensor Fields – Advances and Perspectives*, pages 263–280. Springer, 2009.
- 96 S. M. Pizer, C. A. Burbeck, J. M. Coggins, D. S. Fritsch, and B. S. Morse. Object shape before boundary shape: Scale-space medial axes. *Journal of Mathematical Imaging and Vision*, 4:303–313, 1994.
- 97 F. H. Post, B. Vrolijk, H. Hauser, R. S. Laramée, and H. Doleisch. The state of the art in flow visualisation: Feature extraction and tracking. *Computer Graphics Forum*, 22(4):775–792, 2003.

- 98 B. Preim and D. Bartz. *Visualization in Medicine. Theory, Algorithms, and Applications*. Morgan Kaufmann, 2007.
- 99 M. Rousson, T. Brox, and R. Deriche. Active unsupervised texture segmentation on a diffusion based feature space. In *IEEE Conference on Computer Vision and Pattern Recognition (CVPR)*, pages 699–706, 2003.
- 100 M. Rousson, C. Lenglet, and R. Deriche. Level set and region based surface propagation for diffusion tensor MRI segmentation. In M. Šonka, I. A. Kakadiaris, and J. Kybic, editors, *Computer Vision and Mathematical Methods in Medical and Biomedical Image Analysis*, volume 3117 of *LNCS*, pages 123–134. Springer, 2004.
- 101 T. Salzbrunn and G. Scheuermann. Streamline predicates. *IEEE Transactions on Visualization and Computer Graphics*, 12(6):1601–1612, 2006.
- 102 P. Savadjiev, J. S. Campbell, G. B. Pike, and K. Siddiqi. Streamline flows for white matter fibre pathway segmentation in diffusion MRI. In D. Metaxas et al., editor, *Proc. Medical Image Computing and Computer-Assisted Intervention (MICCAI)*, volume 5241 of *LNCS*, pages 135–143. Springer, 2008.
- 103 G. Scheuermann and X. Tricoche. Topological methods in flow visualization. In C. Johnson and C. Hansen, editors, *The Visualization Handbook*, pages 341–356. Academic Press, 2004.
- 104 V. J. Schmithorst, M. Wilke, B. J. Dardzinski, and S. K. Holland. Cognitive functions correlate with white matter architecture in a normal pediatric population: A diffusion tensor MRI study. *Human Brain Mapping*, 26(2):139–147, 2005.
- 105 T. Schultz. *Feature Extraction for Visual Analysis of DW-MRI Data*. PhD thesis, Universität des Saarlandes, Germany, 2009.
- 106 T. Schultz, B. Burgeth, and J. Weickert. Flexible segmentation and smoothing of DT-MRI fields through a customizable structure tensor. In G. Bebis et al., editor, *Advances in Visual Computing (Proc. ISVC)*, volume 4291 of *LNCS*, pages 455–464, 2006.
- 107 T. Schultz, N. Sauber, A. Anwender, H. Theisel, and H.-P. Seidel. Virtual Klingler dissection: Putting fibers into context. *Computer Graphics Forum (Proc. EuroVis)*, 27(3):1063–1070, 2008.
- 108 T. Schultz and H.-P. Seidel. Estimating crossing fibers: A tensor decomposition approach. *IEEE Transactions on Visualization and Computer Graphics (Proc. IEEE Visualization)*, 14(6):1635–1642, 2008.
- 109 T. Schultz and H.-P. Seidel. Using eigenvalue derivatives for edge detection in DT-MRI data. In G. Rigoll, editor, *Pattern Recognition (Proc. DAGM)*, volume 5096 of *LNCS*, pages 193–202. Springer, 2008.
- 110 T. Schultz, H. Theisel, and H.-P. Seidel. Segmentation of DT-MRI anisotropy isosurfaces. In K. Museth, T. Möller, and A. Ynnerman, editors, *Proc. Eurographics/IEEE-VGTC Symposium on Visualization (EuroVis) 2007*, pages 187–194, 2007.
- 111 T. Schultz, H. Theisel, and H.-P. Seidel. Topological visualization of brain diffusion MRI data. *IEEE Transactions on Visualization and Computer Graphics (Proc. IEEE Visualization)*, 13(6):1496–1503, 2007.
- 112 T. Schultz, H. Theisel, and H.-P. Seidel. Crease surfaces: From theory to extraction and application to diffusion tensor MRI. *IEEE Transactions on Visualization and Computer Graphics*, 16(1):109–119, 2010.
- 113 J. A. Sethian. *Level Set Methods and Fast Marching Methods*. Cambridge University Press, 2nd edition, 2001.
- 114 A. Sherbondy, D. Akers, R. Mackenzie, R. Dougherty, and B. Wandell. Exploring connectivity of the brain’s white matter with dynamic queries. *IEEE Transactions on Visualization and Computer Graphics*, 11(4):419–430, 2005.
- 115 J. Shi and J. Malik. Normalized cuts and image segmentation. *IEEE Transactions on Pattern Analysis and Machine Intelligence*, 22(8):888–905, 2000.

- 116 J. S. Shimony, A. Z. Snyder, N. Lori, and T. E. Conturo. Automated fuzzy clustering of neuronal pathways in diffusion tensor tracking. In *Proc. International Society of Magnetic Resonance in Medicine (ISMRM)*, volume 10, 2002.
- 117 S. M. Smith, M. Jenkinson, H. Johansen-Berg, D. Rueckert, T. E. Nichols, C. E. Mackay, K. E. Watkins, O. Ciccarelli, M. Z. Cader, P. M. Matthews, and T. E. J. Behrens. Tract-based spatial statistics: Voxelwise analysis of multi-subject diffusion data. *NeuroImage*, 31(4):1487–1505, 2006.
- 118 J.-D. Tournier, F. Calamante, D. G. Gadian, and A. Connelly. Direct estimation of the fiber orientation density function from diffusion-weighted MRI data using spherical deconvolution. *NeuroImage*, 23:1176–1185, 2004.
- 119 X. Tricoche. *Vector and Tensor Field Topology Simplification, Tracking, and Visualization*. PhD thesis, Fachbereich Informatik, Universität Kaiserslautern, 2002.
- 120 X. Tricoche, G. Kindlmann, and C.-F. Westin. Invariant crease lines for topological and structural analysis of tensor fields. *IEEE Transactions on Visualization and Computer Graphics (Proc. IEEE Visualization)*, 14(6):1627–1634, 2008.
- 121 A. Tsai, C.-F. Westin, A. O. Hero III, and A. S. Willsky. Fiber tract clustering on manifolds with dual rooted-graphs. In *Proc. IEEE Conference on Computer Vision and Pattern Recognition (CVPR)*, 2007.
- 122 D. S. Tuch. Q-Ball imaging. *Magnetic Resonance in Medicine*, 52:1358–1372, 2004.
- 123 A. Vilanova, S. Zhang, G. Kindlmann, and D. H. Laidlaw. An introduction to visualization of diffusion tensor imaging and its applications. In J. Weickert and H. Hagen, editors, *Visualization and Processing of Tensor Fields*, pages 121–153. Springer, 2006.
- 124 A. N. Voineskos, L. J. O’Donnell, N. J. Lobaugh, D. Markant, S. H. Ameis, M. Niethammer, B. H. Mulsant, B. G. Pollock, J. L. Kennedy, C.-F. Westin, and M. E. Shenton. Quantitative examination of a novel clustering method using magnetic resonance diffusion tensor tractography. *NeuroImage*, 45(2):370–376, 2009.
- 125 Z. Wang and B. C. Vemuri. An affine invariant tensor dissimilarity measure and its applications to tensor-valued image segmentation. In *Proc. IEEE Conf. on Computer Vision and Pattern Recognition (CVPR)*, volume 1, pages 228–233, 2004.
- 126 Z. Wang and B. C. Vemuri. DTI segmentation using an information theoretic tensor dissimilarity measure. *IEEE Transactions on Medical Imaging*, 24(10):1267–1277, 2005.
- 127 D. Wassermann, M. Descoteaux, and R. Deriche. Diffusion maps segmentation of magnetic resonance q-ball imaging. In *Proc. IEEE International Conference on Computer Vision (ICCV)*, 2007.
- 128 T. Weinkauff. *Extraction of Topological Structures in 2D and 3D Vector Fields*. PhD thesis, Fakultät für Informatik, Otto-von-Guericke-Universität Magdeburg, 2008.
- 129 Y. Weiss. Segmentation using eigenvectors: A unifying view. In *Proc. IEEE International Conference on Computer Vision (ICCV)*, pages 975–982, 1999.
- 130 Y. T. Weldeslassie and G. Hamarneh. DT-MRI segmentation using graph cuts. In J. P. W. Pluim and J. M. Reinhardt, editors, *Medical Imaging 2007: Image Processing*, volume 6512 of *Proc. SPIE*, page 65121K, 2007.
- 131 C.-F. Westin, S. Maier, B. Khidhir, P. Everett, F. Jolesz, and R. Kikinis. Image processing for diffusion tensor magnetic resonance imaging. In *Proc. Medical Image Computing and Computer-Assisted Intervention (MICCAI)*, volume 1679 of *LNCS*, pages 441–452. Springer, 1999.
- 132 C.-F. Westin, S. Maier, H. Mamata, A. Nabavi, F. Jolesz, and R. Kikinis. Processing and visualization for diffusion tensor MRI. *Medical Image Analysis*, 6:93–108, 2002.
- 133 M. R. Wiegell, D. Tuch, H. B. Larsson, and V. J. Wedeen. Automatic segmentation of thalamic nuclei from diffusion tensor magnetic resonance imaging. *NeuroImage*, 19:391–401, 2003.

- 134 B. P. Witwer, R. Moftakhar, K. M. Hasan, P. Deshmukh, V. Haughton, A. Field, K. Arfanakis, J. Noyes, C. H. Moritz, E. Meyerand, H. A. Rowley, A. L. Alexander, and B. Badie. Diffusion-tensor imaging of white matter tracts in patients with cerebral neoplasm. *Journal of Neurosurgery*, 97:568–575, 2002.
- 135 Y. Xia, A. U. Turken, S. L. Whitfield-Gabrieli, and J. D. Gabrieli. Knowledge-based classification of neuronal fibers in entire brain. In J. Duncan and G. Gerig, editors, *Proc. Medical Image Computing and Computer-Assisted Intervention (MICCAI)*, volume 3749 of *LNCS*, pages 205–212. Springer, 2005.
- 136 R. Xu. *Clustering*. Wiley, 2009.
- 137 P. A. Yushkevich, H. Zhang, T. J. Simon, and J. C. Gee. Structure-specific statistical mapping of white matter tracts. *NeuroImage*, 41:448–461, 2008.
- 138 S. Zhang, S. Correia, and D. H. Laidlaw. Identifying white-matter fiber bundles in DTI data using an automated proximity-based fiber-clustering method. *IEEE Transactions on Visualization and Computer Graphics*, 14(5):1044–1053, 2008.
- 139 S. Zhang, C. Demiralp, and D. H. Laidlaw. Visualizing diffusion tensor MR images using streamtubes and streamsurfaces. *IEEE Transactions on Visualization and Computer Graphics*, 9(4):454–462, 2003.
- 140 S. Zhang, D. H. Laidlaw, and G. Kindlmann. Diffusion tensor MRI visualization. In C. D. Hansen and C. R. Johnson, editors, *The Visualization Handbook*, pages 327–340. Elsevier, 2005.
- 141 X. Zheng and A. Pang. HyperLIC. In *Proc. IEEE Visualization*, pages 249–256, 2003.
- 142 X. Zheng, B. Parlett, and A. Pang. Topological lines in 3D tensor fields and discriminant hessian factorization. *IEEE Transactions on Visualization and Computer Graphics*, 11(4):395–407, 2005.
- 143 X. Zheng, X. Tricoche, and A. Pang. Degenerate 3D tensors. In J. Weickert and H. Hagen, editors, *Visualization and Processing of Tensor Fields*, pages 241–256. Springer, 2006.
- 144 L. Zhukov, K. Museth, D. Breen, R. Whitaker, and A. H. Barr. Level set segmentation and modeling of DT-MRI human brain data. *Journal of Electronic Imaging*, 12:125–133, 2003.
- 145 U. Ziyang, D. Tuch, and C.-F. Westin. Segmentation of thalamic nuclei from DTI using spectral clustering. In R. Larsen, M. Nielsen, and J. Sporring, editors, *Proc. Medical Image Processing and Computer-Assisted Intervention (MICCAI)*, volume 4191 of *LNCS*, pages 807–814. Springer, 2006.
- 146 U. Ziyang and C.-F. Westin. Joint segmentation of thalamic nuclei from a population of diffusion tensor MR images. In D. Metaxas, L. Axel, G. Fichtinger, and G. Székely, editors, *Proc. Medical Image Processing and Computer-Assisted Intervention (MICCAI)*, volume 5241 of *LNCS*, pages 279–286. Springer, 2008.